Journal of Materials Chemistry A

Materials for energy and sustainability

rsc.li/materials-a
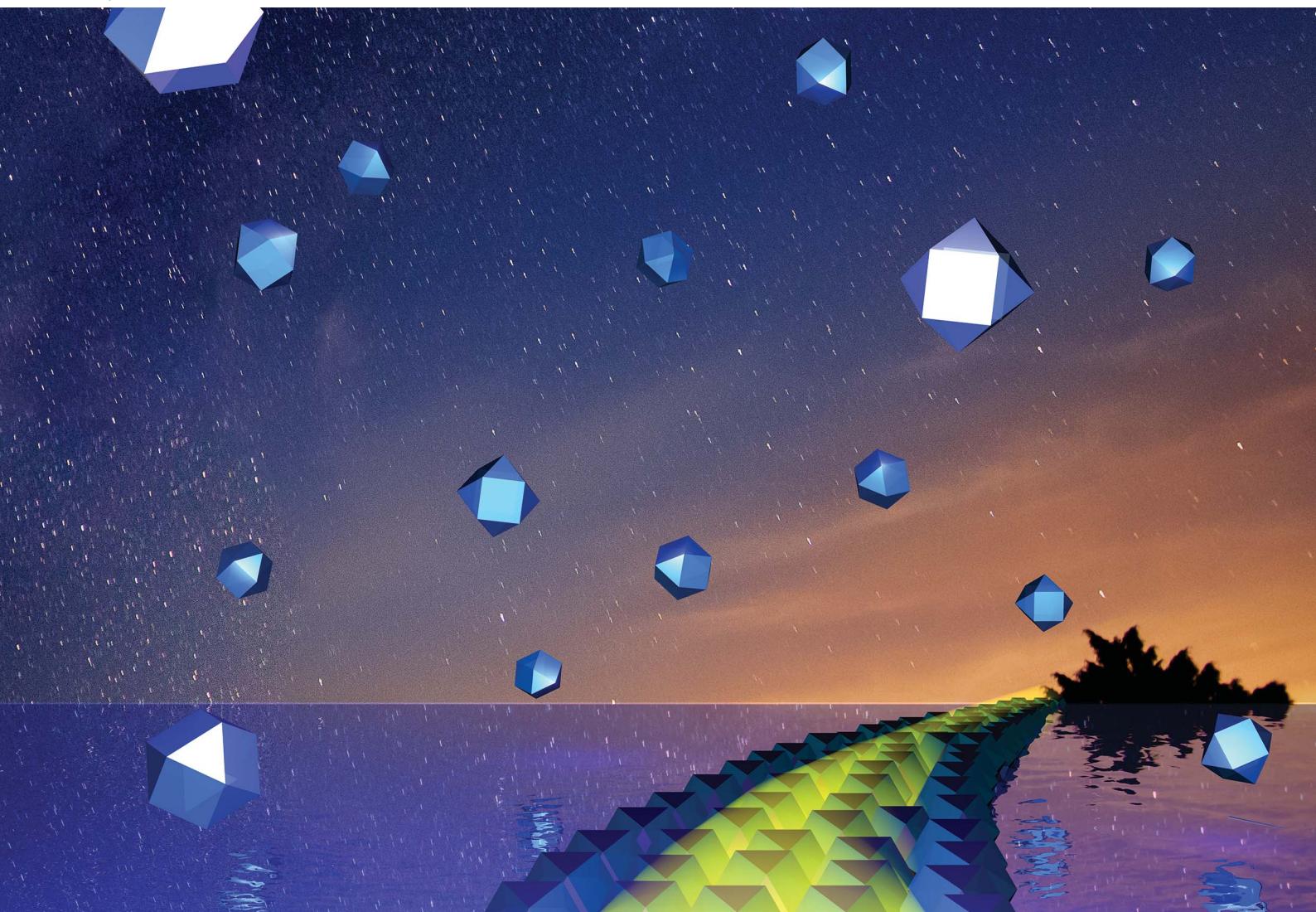
Themed issue: Emerging Investigators 2021

ROYAL SOCIETY
OF CHEMISTRY

COMMUNICATION
Kenji Okada, Masahide Takahashi *et al.*
Oriented growth of semiconducting TCNQ@Cu_3(BTC)$_2$
MOF on Cu(OH)$_2$: crystallographic orientation and pattern
formation toward semiconducting thin-film devices

Check for updates

Oriented growth of semiconducting TCNQ@Cu₃(BTC)₂ MOF on Cu(OH)₂: crystallographic orientation and pattern formation toward semiconducting thin-film devices†

Kenji Okada, [ID] *[ab] Keyaki Mori,[a] Arisa Fukatsu [ID] [a] and Masahide Takahashi [ID] *[a]

The host–guest system TCNQ@Cu₃(BTC)₂ (TCNQ = 7,7,8,8-tetra-cyanoquinodimethane, BTC = 1,3,5-benzenetricarboxylate) exhibits semiconducting properties with potential applications in thin-film devices, such as field-effect transistors and thermoelectric films. Although controlling its crystallographic orientation is important for the efficient use of its electrical properties in advanced semi-conductors, the fabrication of $Cu_3(BTC)_2$ thin films with both in-plane and out-of-plane orientations (three-dimensionally oriented thin films) remains a challenge. Here, we report on the fabrication of three-dimensionally oriented $Cu_3(BTC)_2$ thin films *via* heteroepitaxial growth on $Cu(OH)_2$. The epitaxial growth direction of $Cu_3(BTC)_2$ is determined by lattice matching at the $Cu_3(BTC)_2/Cu(OH)_2$ interface and interface bonding (local chemical connection matching; spatial matching of Cu atoms across the interface). The epitaxial growth approach enables the fabrication of oriented TCNQ@Cu₃(BTC)₂ thin films, where the {111} lattice plane, which can be a conducting path, is oriented both parallel and perpendicular to the substrate. Owing to the in-plane orientation of the {111} lattice plane in the oriented TCNQ@Cu₃(BTC)₂ film, we have, for the first time, achieved MOF thin films with anisotropic electrical properties in the in-plane direction. Moreover, we show that it is possible to fabricate oriented MOF patterns by integration with UV lithography technology. The oriented MOF patterns with anisotropic conduction will pave the way for next-generation smart electronic devices.

1. Introduction

Metal–organic frameworks (MOFs), also called porous coordination polymers, are crystalline porous organic–inorganic hybrid materials consisting of metal-based nodes and organic linkers *via* coordination bonds.[1,2] Because of their periodic frameworks as well as structural and chemical versatility, MOFs are being developed for bulk applications, such as gas storage and engineering operations (catalysis, separation).[3–6] More recently, the potential applications of MOFs have focused on high-value technological areas (*e.g.*, thin-film devices) because of their "designable" electrical properties that benefit from the ordered micropores and frameworks, and are unprecedented in other materials. These include short- and long-range ordered micropores, metal-based nodes and organic linkers, and versatile host–guest chemistry ("guest@MOF" properties), as introduced in recent review articles.[7–12] However, most MOFs exhibit poor electrical conductivity because of the insulating organic ligands and poor overlap between the atomic orbitals of metal ions. In 2014, Talin *et al.* reported a promising host–guest system that affects the electrical conductivity of MOFs. The infiltration of insulating $Cu_3(BTC)_2$ MOF (also known as HKUST-1, BTC = 1,3,5-benzenetricarboxylate) by the redox-active guest molecule 7,7,8,8-tetracyanoquinodimethane (TCNQ) (TCNQ@Cu₃(BTC)₂) increased its conductivity by six orders of magnitude from 10^{-8} to 0.07 S cm^{-1}.[13] It was proposed that conducting pathways were formed in TCNQ@Cu₃(BTC)₂ when TCNQ bridged the two neighbouring Cu-paddlewheels.[13] Its semiconducting properties make TCNQ@Cu₃(BTC)₂ a novel and promising material for thin-film devices, such as micro-electronic devices, sensors, and thermoelectric devices.[14–16] The conducting path is known to exist along the {111} lattice plane of TCNQ@Cu₃(BTC)₂; this is supported by both theoretical and experimental data.[13,17] Therefore, a key concern is the fabrication of thin films with controlled orientation, especially {111} lattice planes of $Cu_3(BTC)_2$, for sophisticated thin-film devices. The use of substrates modified with self-assembled monolayers (SAMs) is one of the most widely used methods for fabricating oriented MOF thin films.[18–21] In this method, the lattice plane parallel to the substrate (out-of-plane orientation) can be controlled by changing the terminated functional group of the SAM. In fact, in semiconducting TCNQ@Cu₃(BTC)₂ thin films for thin-film devices reported so far, an SAM-modified

[a]*Department of Materials Science, Graduate School of Engineering, Osaka Prefecture University, Sakai, Osaka, 599-8531, Japan. E-mail: k_okada@mtr.osakafu-u.ac.jp; masa@mtr.osakafu-u.ac.jp*

[b]*JST, PRESTO, 4-1-8 Honcho, Kawaguchi, Saitama, 332-0012, Japan*

† Electronic supplementary information (ESI) available. See DOI: 10.1039/d1ta02968a

This journal is © The Royal Society of Chemistry 2021

J. Mater. Chem. A, 2021, 9, 19613–19618 | 19613

substrate is employed to fabricate the oriented $Cu_3(BTC)_2$ thin film, in which the {111} lattice plane is preferentially oriented parallel to the substrate.[13,22,23] However, although existing methods can control the crystallographic orientation along the out-of-plane direction (perpendicular to the substrate), $Cu_3(BTC)_2$ thin films with both out-of-plane and in-plane (parallel to the substrate) orientations have not been achieved. The fabrication of $Cu_3(BTC)_2$ thin films with both out-of-plane and in-plane orientations is an important step towards realizing MOF-based thin-film devices, as is the case with inorganic material-based semiconductors.

The fabrication of $Cu_3(BTC)_2$ thin films with both out-of-plane and in-plane orientations is difficult compared with MOFs with low crystal symmetry (lattice anisotropy, *e.g.* NU-1000: $P6/mmm$), whose crystals usually exhibit an anisotropic morphology, such as nanorods and nanosheets.[24] Because the $Cu_3(BTC)_2$ crystal is isotropic owing to its high crystal symmetry ($Fm\bar{3}m$), it is difficult to orient the crystallites towards a specific direction even when external fields (*e.g.* share force, electric, and magnetic fields) are applied. Therefore, it is scientifically challenging to fabricate $Cu_3(BTC)_2$ thin films with both out-of-plane and in-plane orientations. In the present study, we have, for the first time, successfully fabricated $Cu_3(BTC)_2$ thin films with both out-of-plane and in-plane orientations by employing an epitaxial growth approach on $Cu(OH)_2$ that we developed.[25–29] Both the lattice matching at the $Cu_3(BTC)_2$/$Cu(OH)_2$ interface and the interface bonding (local chemical connection matching; spatial matching of Cu atoms across the interface) allow the crystallographic orientation of $Cu_3(BTC)_2$. The epitaxial growth approach enables the fabrication of oriented $TCNQ@Cu_3(BTC)_2$ thin films, where the {111} lattice plane, which can be a conducting path, is oriented both parallel and perpendicular to the substrate. Owing to the in-plane orientation of the {111} lattice plane in the oriented $TCNQ@Cu_3(BTC)_2$ thin film, MOF thin films with anisotropic electrical properties in the in-plane direction were obtained for the first time. We also show that it is possible to fabricate oriented MOF patterns by integration with UV lithography technology. The oriented MOF patterns with anisotropic conduction will pave the way for next-generation smart electronic devices.

2. Results and discussion

2.1 Oriented growth of $Cu_3(BTC)_2$ on $Cu(OH)_2$

Oriented $Cu_3(BTC)_2$ thin films were fabricated on aligned $Cu(OH)_2$ nanobelts *via* a one-pot method, in which $Cu(OH)_2$ nanobelts oriented on Si substrates were reacted with H_3BTC in a water–ethanol mixture (1 : 1 vol%) at room temperature for 10 min. After the reaction, homogeneous $Cu_3(BTC)_2$ thin films were obtained on the entire surface of the centimetre-scale substrate (see Fig. S1†). The surface of $Cu(OH)_2$ nanobelts was covered with cuboctahedron-shaped crystals, which were observed as $Cu_3(BTC)_2$ crystals (Fig. 1a).[30] The triangular and square shapes (some missing edges) on the exposed surface of the crystals indicate the {111} and {100} facets, respectively. A cross-sectional scanning electron microscope (SEM) image
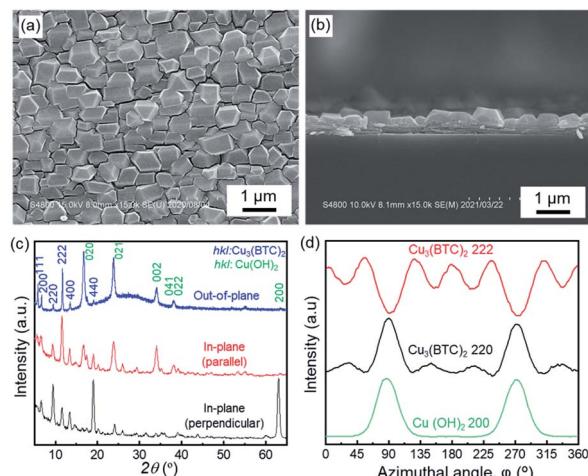
Fig. 1 SEM images ((a) top view and (b) cross-section) of the oriented $Cu_3(BTC)_2$ thin film (the longitudinal direction (*a*-axis) of the underlying $Cu(OH)_2$ nanobelts is aligned horizontal to the images). (c) XRD patterns of the oriented $Cu_3(BTC)_2$ thin film. Three setups for the XRD investigations were used: out-of-plane (blue line), in-plane (red and black line; X-ray incident angle is parallel, and perpendicular to longitudinal direction of nanobelts at $\varphi = 0°$). (d) Azimuthal angle dependence of intensity (φ scan) profiles of the 222 and 220 reflections of $Cu_3(BTC)_2$ and 200 reflection of $Cu(OH)_2$ (X-ray incident angle is parallel to longitudinal direction (*a*-axis) of $Cu(OH)_2$ nanobelts at $\varphi = 0°$).

showed that $Cu_3(BTC)_2$ thin films with a thickness of ~300 nm formed on the $Cu(OH)_2$ nanobelt film, and that $Cu_3(BTC)_2$ crystallites were connected to each other (Fig. 1b). Because of the isotropic morphologies of $Cu_3(BTC)_2$ crystals, it is difficult to confirm their orientation by SEM images (we can observe the orientation when we focus on the triangular {111} and square {100} facets). The crystallographic structure and orientation of $Cu_3(BTC)_2$ were confirmed by X-ray diffraction (XRD) experiments using previously reported protocols, which allow the crystallographic orientation along all three axes to be examined (Fig. 1c).[25–29] The diffraction patterns can be attributed to $Cu_3(BTC)_2$ and $Cu(OH)_2$ (see Fig. S2†). The intense 222 reflection of $Cu_3(BTC)_2$ in the out-of-plane XRD pattern (at $2\theta = 11.7°$) compared with the powder XRD pattern indicates that the {111} lattice planes of the MOF were preferentially oriented parallel to the substrate. Most reflections, especially 220 and 222 reflections (at $2\theta = 9.5°$ and $11.7°$, respectively) detected in both in-plane XRD measurements, show a distinct X-ray incident angular dependence. These results indicate that the {110} and {111} lattice planes of the MOF crystals are aligned orthogonally to each other over the entire surface, and perpendicularly to the substrate. More detailed in-plane orientations of the {110} and {111} lattice planes were investigated by considering the azimuthal angle dependence of the intensity (φ scan) profiles (Fig. 1d). This method provides information on the angular relationship between the selected lattice planes of $Cu_3(BTC)_2$ and $Cu(OH)_2$ in the in-plane direction. Intense signals were detected at $\varphi = 90°$ and $\varphi = 270°$ for the 200 and 220 reflections of $Cu(OH)_2$ and $Cu_3(BTC)_2$, respectively, whereas 222 reflections

19614 | *J. Mater. Chem. A*, 2021, **9**, 19613–19618

This journal is © The Royal Society of Chemistry 2021

of $Cu_3(BTC)_2$ were detected at approximately $\varphi = 0$, 55, 125, 180, 235, 305 and 360°, showing strong angular dependence. The φ scan profiles clearly indicate that the {110} lattice planes of $Cu_3(BTC)_2$ are parallel to the {100} lattice planes of $Cu(OH)_2$. On the other hand, the {111} lattice planes of $Cu_3(BTC)_2$ are orthogonal to the {100} lattice planes of $Cu(OH)_2$, and at an angle of approximately $\pm35°$ to the {100} lattice planes of $Cu(OH)_2$, with the rotational axis perpendicular to the substrate. The epitaxial relationship was further confirmed by an in-plane reciprocal space map (see Fig. S3†). The detailed analysis of the XRD results revealed that $Cu_3(BTC)_2$ crystals epitaxially grown under two different types of orientation relationships coexist in the oriented film, i.e. $Cu_3(BTC)_2$ epitaxially grown with either the {111} lattice planes or the {100} lattice planes parallel to the longitudinal direction (a-axis) of $Cu(OH)_2$ nanobelts (Fig. 2a, b and S4†). The former orientation relationship is described as $[11\bar{1}](112)Cu_3(BTC)_2//[001](010)Cu(OH)_2$, and the latter as $[001](110)Cu_3(BTC)_2//[001](010)Cu(OH)_2$. In both orientation relationships, the (110) lattice planes of $Cu_3(BTC)_2$ are perpendicular to the a-axis of $Cu(OH)_2$; this is supported by the similar φ scan profiles of the 220 and 200 reflections of $Cu_3(BTC)_2$ and $Cu(OH)_2$, respectively. In the $[11\bar{1}](112)Cu_3(BTC)_2//[001](010)$ $Cu(OH)_2$ orientation relationship, the {111} lattice planes of $Cu_3(BTC)_2$ are parallel to the a-axis of $Cu(OH)_2$, and perpendicular to the substrate. In contrast, in the $[001](110)$ $Cu_3(BTC)_2//[001](010)Cu(OH)_2$ orientation relationship, the {111} lattice planes of $Cu_3(BTC)_2$ are at an angle of approximately $\pm35°$ to the c-axis of $Cu(OH)_2$, with the rotational axis perpendicular to the substrate. These results are in good agreement with the φ scan measurements. The peaks at $\varphi = 0$, 180, and 360° in the φ scan profile of the 222 reflection can be attributed to the $[11\bar{1}](112)Cu_3(BTC)_2//[001](010)Cu(OH)_2$ orientation relationship. The peaks at $\varphi = 55$, 125, 235, and 305° can be attributed to the $[001](110)Cu_3(BTC)_2//[001](010)$

$Cu(OH)_2$ orientation relationship. In addition, the $Cu_3(BTC)_2$ crystals epitaxially grown in the two different types of orientation relationships were observed in the SEM images (Fig. 2c and d). Notably, the {111} lattice planes, which can be conducting paths in $TCNQ@Cu_3(BTC)_2$, were present both parallel and perpendicular to the substrate. The {111} lattice planes perpendicular to the substrate showed a strong angular dependence in the in-plane direction (see Fig. S5†). This is the first report showing the three-dimensionally crystallographic orientation of $Cu_3(BTC)_2$ thin films, especially the important {111} lattice planes in $TCNQ@Cu_3(BTC)_2$.

The orientation of $Cu_3(BTC)_2$ can be explained by the epitaxial growth on $Cu(OH)_2$. As revealed by the XRD investigation, $Cu_3(BTC)_2$ crystals epitaxially grow under two different types of orientation relationships: $[11\bar{1}](112)Cu_3(BTC)_2//[001](010)Cu(OH)_2$ and $[001](110)Cu_3(BTC)_2//[001](010)$ $Cu(OH)_2$. The key to the epitaxial growth of $Cu_3(BTC)_2$ in the orientation relationships is the interface bonding (local chemical connection matching; spatial matching of Cu atoms across the $Cu_3(BTC)_2/Cu(OH)_2$ interface). If only the lattice mismatch is considered, then better orientation relationships (e.g. $[010](100)Cu_3(BTC)_2//[001](010)Cu(OH)_2$ with 0.68%) are obtained; however, these orientations were not confirmed. It is important to note that, in the two different types of orientation relationships observed in the present work, the Cu–Cu in the Cu-paddlewheel units in $Cu_3(BTC)_2$ is parallel to a-axis of $Cu(OH)_2$ at the interface (see Fig. S6 and S7†). The Cu–Cu distance of the Cu-paddlewheel units in $Cu_3(BTC)_2$ is approximately 2.63 Å, which is in good agreement with the distance between Cu atoms along the a-axis of $Cu(OH)_2$ (2.95 Å). This allows the formation of coordination bonds between $Cu(OH)_2$ and the carboxylic acid of the BTC linker at the $Cu_3(BTC)_2/$ $Cu(OH)_2$ interface. Other orientation relationships are unsuitable for forming coordination bonds with the carboxylic acid owing to the large distances between Cu atoms. The bond formation requirement at the interface results in the alignment of Cu-paddlewheel units parallel to the a-axis of $Cu(OH)_2$. In both orientation relationships, the lattice mismatch was sufficiently small for epitaxial growth: 5.34% for $[11\bar{1}](112)$ $Cu_3(BTC)_2//[001](010)Cu(OH)_2$ and 5.34% for $[001](110)$ $Cu_3(BTC)_2//[001](010)Cu(OH)_2$. Both lattice matching at the interface and interface bonding were found to be important for the epitaxial growth of MOFs. The epitaxial growth conditions of MOFs, considering both lattice matching at the interface and interface bonding, have recently been considered in the field of MOF epitaxial growth, such as single crystal MOF-on-MOF systems, and our computational study on the epitaxial growth of Cu-based MOFs on $Cu(OH)_2$.[31,32]

Fig. 2 Schematics and SEM images of the $Cu_3(BTC)_2$ crystals epitaxially grown under $[11\bar{1}](112)Cu_3(BTC)_2//[001](010)Cu(OH)_2$ (a and c) and $[001](110)Cu_3(BTC)_2//[001](010)Cu(OH)_2$ (b and d) orientation relationships. The cuboctahedron-shaped crystals and green rectangles denote the $Cu_3(BTC)_2$ crystals and $Cu(OH)_2$ nanobelts, respectively. In the SEM images, the longitudinal direction (a-axis) of the underlying $Cu(OH)_2$ nanobelts is aligned horizontal to the images.

2.2 Oriented $Cu_3(BTC)_2$ patterns

The development of a novel method to precisely control both the crystallographic orientation of MOFs and the MOF position on substrates is a fundamental step towards exploiting the unique properties of MOFs in miniaturised devices, such as lab-on-a-chip or microfluidic devices.[33] Among the different approaches (e.g. the use of pre-patterned SAM), the fabrication

This journal is © The Royal Society of Chemistry 2021

J. Mater. Chem. A, 2021, 9, 19613–19618 | 19615

of MOF patterns by photolithography used in current micro-fabrication technology is a promising method because of the formation of high-resolution MOF patterns and compatibility with existing semiconductor fabrication processes.[18,34–37] Although photolithography techniques can efficiently prepare precise MOF patterns, the fabrication of MOF patterns with crystallographic orientation (oriented MOF patterns) by integration with conventional lithography technology remains a challenge. In particular, the oriented MOF patterns of semiconducting TCNQ@$Cu_3(BTC)_2$ contribute to the development of MOF-based thin-film devices. The present approach, which uses $Cu(OH)_2$ nanoassemblies as a support for MOF growth, offers advantages in terms of the MOF orientation and the formation of MOF thin films and patterns on various substrates.[38–40] Here, we show for the first time the fabrication of oriented MOF patterns with micrometre-scale resolution in combination with conventional photolithography techniques (Fig. 3). Fabrication was conducted using the following process. The photoresist patterns were fabricated on a Si wafer using a standard UV lithography method. The oriented $Cu(OH)_2$ thin film was

deposited onto the Si wafer with the photoresist patterns. The photoresist patterns were then removed by ultrasonic treatment in acetone. The resulting oriented $Cu(OH)_2$ patterns were converted into oriented $Cu_3(BTC)_2$ patterns. The orientation of the $Cu_3(BTC)_2$ patterns was confirmed by XRD (see Fig. S8†). No pattern detachment was observed during the conversion process. Oriented MOF patterns that finely transferred the photomask patterns were obtained. By using a higher resolution photoresist pattern, it will be possible to form an oriented MOF pattern with a higher resolution. As the width of the $Cu(OH)_2$ nanobelt is approximately 50 nm, the fabrication of oriented MOF patterns with a resolution of up to 50 nm is possible by combination with recently developed microfabrication technology.

2.3 Anisotropic conductivity of the oriented TCNQ@$Cu_3(BTC)_2$ film

The electrical conductivity of oriented $Cu_3(BTC)_2$ thin films infiltrated with TCNQ was investigated (Fig. 4 and see Fig. S9†). The infiltration of TCNQ into the oriented $Cu_3(BTC)_2$ thin film was conducted as follows. First, the oriented $Cu_3(BTC)_2$ thin film prepared on polyimide was placed in a borosilicate glass tube and desolvated under high vacuum ($\sim10^{-4}$ Pa) at 180 °C for 3 h. The film was removed from the borosilicate glass tube, placed in a glove bag filled with N_2 gas, and immersed in a saturated TCNQ solution in dichloromethane for three days. After three days, the TCNQ@$Cu_3(BTC)_2$ was washed twice with dichloromethane and then air-dried. By changing the orientation of the underlying $Cu(OH)_2$ nanobelts on the substrate, the directional relationship between the {111} lattice planes of TCNQ@$Cu_3(BTC)_2$ and the direction of electrical measurements (position of the Pt electrodes) can be defined. The conductivity in the direction parallel and vertical to the {111} lattice planes of TCNQ@$Cu_3(BTC)_2$ were compared by a two-probe method. Electrical measurements showed that the thin film exhibited
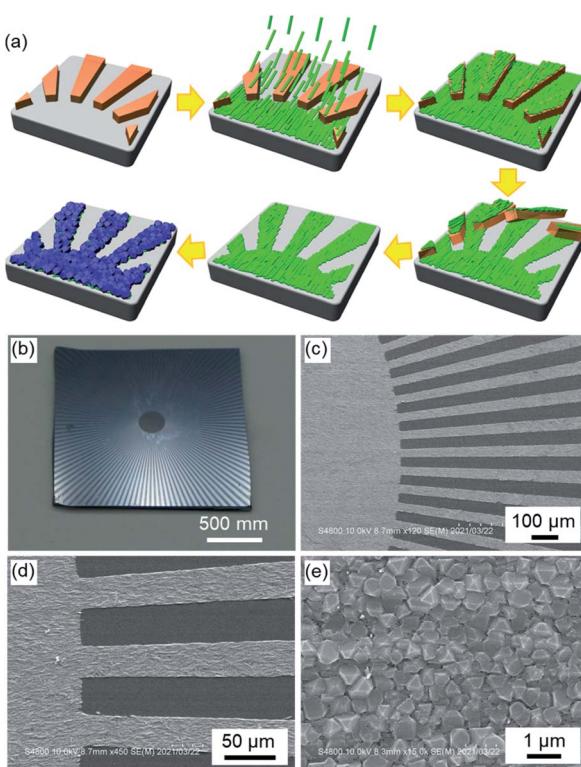
Fig. 3 Fabrication of oriented $Cu_3(BTC)_2$ MOF patterns. (a) Schematics showing the fabrication process. The photoresist patterns (orange blocks) were fabricated on the Si wafer using a standard UV lithography method. The $Cu(OH)_2$ (green rectangles) oriented thin film was deposited onto the Si wafer with the photoresist patterns. The photoresist patterns on which $Cu(OH)_2$ was deposited were removed by ultrasonic treatment in acetone. The resulting oriented $Cu(OH)_2$ patterns were converted into oriented $Cu_3(BTC)_2$ (blue cuboctahedron-shaped crystal) patterns. (b–e) Photo and SEM images of the oriented $Cu_3(BTC)_2$ patterns. In this film, the longitudinal direction (a-axis) of the underlying $Cu(OH)_2$ nanobelts is aligned horizontal to the images.
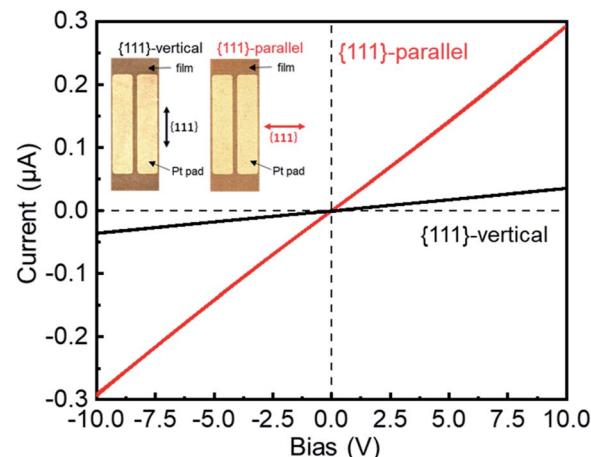
Fig. 4 I–V curves of the oriented TCNQ@$Cu_3(BTC)_2$ thin films on polyimide substrates (Pt pads were 100 μm apart from each other). Electrical measurements were carried out parallel to the {111} lattice plane ({111}-parallel) and vertical to the {111} lattice plane ({111}-vertical).

ohmic behaviour. Its electrical conductivity was approximately 10 times higher in the direction parallel to the {111} lattice planes ($\sim3.2 \times 10^{-3}$ S m^{-1}) compared with the direction perpendicular to the {111} lattice planes ($\sim3.9 \times 10^{-4}$ S m^{-1}). The underlying Cu(OH)$_2$ nanobelt film showed 1000 times lower conductivity than the TCNQ@Cu$_3$(BTC)$_2$ thin film (Fig. S10†), indicating that the anisotropic conductivity is attributed to TCNQ@Cu$_3$(BTC)$_2$. TCNQ molecules are known to preferentially align along the {111} lattice planes of Cu$_3$(BTC)$_2$ MOFs by bridging the coordination motif to two neighbouring Cu-paddlewheels (see Fig. S11†).[13,17] Thus, the oriented TCNQ@Cu$_3$(BTC)$_2$ film showed higher conductivity in the {111} direction. Although anisotropic electrical conductivity and exciton migration have been reported using single-crystal MOFs,[41,42] these results show, for the first time, the anisotropic conductivity in the in-plane direction over a large area of polycrystalline MOF thin films. The anisotropic conductivity of the thin film is attributed to the angular dependence of the {111} lattice planes, which is the conducting path of TCNQ@Cu$_3$(BTC)$_2$ in the in-plane direction.

The effect of substrate bending on the electrical properties of the oriented TCNQ@Cu$_3$(BTC)$_2$ thin film was also investigated (Fig. 5). The oriented TCNQ@Cu$_3$(BTC)$_2$ thin film prepared on an elastic polyimide substrate was bent until the radius of curvature reached 8.25 mm. However, because of the polycrystalline nature of the thin film, the conductivity did not change significantly from when it was flat. No obvious change was observed between the bending of the substrate perpendicular to the longitudinal direction (a-axis) of the underlying Cu(OH)$_2$ nanobelts and the bending of the substrate perpendicular to the short direction (c-axis) of the underlying Cu(OH)$_2$ nanobelts. This small difference can be attributed to the anisotropic structure of the underlying Cu(OH)$_2$ nanobelts; the flexible Cu(OH)$_2$ nanobelt film against bending of the substrate parallel to the longitudinal direction prevented crack formation in the TCNQ@Cu$_3$(BTC)$_2$ thin film. The fabrication of flexible MOF-based thin films with electrical properties is attributed to the flexibility of the organic–inorganic hybrid material MOFs

and the flexible deformation of thin films consisting of Cu(OH)$_2$ nano-assemblies and TCNQ@Cu$_3$(BTC)$_2$ crystallites against macroscopic structural deformation. Flexible and conductive thin films are more feasible for realistic applications in industry than single crystals. The present method, which does not require a specific substrate (e.g. SAM-modified substrate) for the fabrication of oriented TCNQ@Cu$_3$(BTC)$_2$ thin films, allows for substrate versatility and the formation of semiconducting TCNQ@Cu$_3$(BTC)$_2$ thin films on flexible substrates. These advantages enabled us to show, for the first time, the effect of substrate bending on the electrical properties of TCNQ@Cu$_3$(BTC)$_2$ thin films. This will contribute to the research and development of MOF-based (flexible) thin-film smart device applications, such as transistors and thermoelectric thin films.

3. Conclusions

Three-dimensionally (both in-plane and out-of-plane directions) oriented Cu$_3$(BTC)$_2$ thin films over a large centimetre-scale area were synthesised via epitaxial growth on Cu(OH)$_2$. The epitaxial growth approach enables the fabrication of oriented TCNQ@Cu$_3$(BTC)$_2$ thin films, where the {111} lattice plane, which can be a conducting path, is oriented both parallel and perpendicular to the substrate. The Cu$_3$(BTC)$_2$ crystals were epitaxially grown with two types of orientation relationships: Cu$_3$(BTC)$_2$ epitaxially grown with either the {111} or {100} lattice planes parallel to the a-axis of Cu(OH)$_2$. The orientation relationships were determined not only by the lattice matching between Cu$_3$(BTC)$_2$ and Cu(OH)$_2$, but also by interface bonding (local chemical connection matching; spatial matching of Cu atoms across the interface). The realization of polycrystalline TCNQ@Cu$_3$(BTC)$_2$ thin films with in-plane orientation enables the fabrication of MOF-based thin films with anisotropic electrical properties in the in-plane direction. By combining the epitaxial growth approach on Cu(OH)$_2$ nano-assemblies with UV lithography technology, the fabrication of oriented Cu$_3$(BTC)$_2$ patterns is possible. These semiconducting MOF films and patterns with anisotropic properties will pave the way for next-generation smart electronic devices.

Conflicts of interest

There are no conflicts to declare.

Acknowledgements

Notes and references

1 H. Furukawa, K. E. Cordova, M. O'Keeffe and O. M. Yaghi, Science, 2013, 341, 1230444.
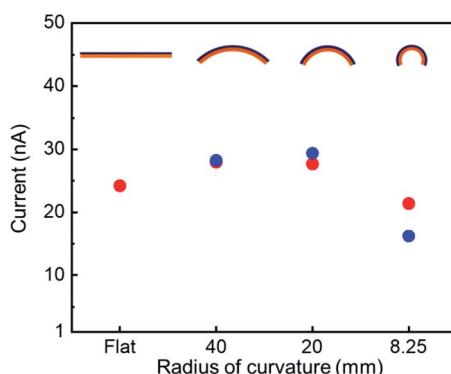
Fig. 5 Current as a function of bending radius of curvature at 10 V (blue circles: bending of a substrate perpendicular to the longitudinal direction (a-axis) of the underlying Cu(OH)$_2$ nanobelts. Red circles: bending of a substrate perpendicular to the short direction (c-axis) of the underlying Cu(OH)$_2$ nanobelts).

This journal is © The Royal Society of Chemistry 2021

J. Mater. Chem. A, 2021, 9, 19613–19618 | 19617

2 S. Kitagawa, R. Kitaura and S.-I. Noro, *Angew. Chem., Int. Ed.*, 2004, **43**, 2334–2375.

3 J. Lee, O. K. Farha, J. Roberts, K. A. Scheidt, S. T. Nguyen and J. T. Hupp, *Chem. Soc. Rev.*, 2009, **38**, 1450–1459.

4 D. Yang and B. C. Gates, *ACS Catal.*, 2019, **9**, 1779–1798.

5 K. Adil, Y. Belmabkhout, R. S. Pillai, A. Cadiau, P. M. Bhatt, A. H. Assen, G. Maurin and M. Eddaoudi, *Chem. Soc. Rev.*, 2017, **46**, 3402–3430.

6 K. Sumida, D. L. Rogow, J. A. Mason, T. M. Mcdonald, E. D. Bloch, Z. R. Herm, T.-H. Bae and J. R. Long, *Chem. Rev.*, 2012, **112**, 724–781.

7 I. Stassen, N. Burtch, A. Talin, P. Falcaro, M. Allendorf and R. Ameloot, *Chem. Soc. Rev.*, 2017, **46**, 3185–3241.

8 L. S. Xie, G. Skorupskii and M. Dincă, *Chem. Rev.*, 2020, **120**, 8536–8580.

9 L. Sun, M. G. Campbell and M. Dincă, *Angew. Chem., Int. Ed.*, 2016, **55**, 3566–3579.

10 C. A. Downes and S. C. Marinescu, *ChemSusChem*, 2017, **10**, 4374–4392.

11 G. Givaja, P. Amo-Ochoa, C. J. Gómez-García and F. Zamora, *Chem. Soc. Rev.*, 2012, **41**, 115–147.

12 L. Sun, S. S. Park, D. Sheberla and M. Dincă, *J. Am. Chem. Soc.*, 2016, **138**, 14772–14782.

13 A. A. Talin, A. Centrone, A. C. Ford, M. E. Foster, V. Stavila, P. Haney, R. A. Kinney, V. Szalai, F. El Gabaly, H. P. Yoon, F. Léonard and M. D. Allendorf, *Science*, 2014, **343**, 66–69.

14 Z. Wang, D. Nminibapiel, P. Shrestha, J. Liu, W. Guo, P. G. Weidler, H. Baumgart, C. Wöll and E. Redel, *ChemNanoMat*, 2016, **2**, 67–73.

15 X. Chen, Z. Wang, Z. M. Hassan, P. Lin, K. Zhang, H. Baumgart and E. Redel, *ECS J. Solid State Sci. Technol.*, 2017, **6**, 150–153.

16 K. J. Erickson, F. Léonard, V. Stavila, M. E. Foster, C. D. Spataru, R. E. Jones, B. M. Foley, P. E. Hopkins, M. D. Allendorf and A. A. Talin, *Adv. Mater.*, 2015, **27**, 3453–3459.

17 C. Schneider, D. Ukaj, R. Koerver, A. A. Talin, G. Kieslich, S. P. Pujari, H. Zuilhof, J. Janek, M. D. Allendorf and R. A. Fischer, *Chem. Sci.*, 2018, **9**, 7405–7412.

18 O. Shekhah, H. Wang, D. Zacher, R. A. Fischer and C. Wöll, *Angew. Chem., Int. Ed.*, 2009, **48**, 5038–5041.

19 O. Shekhah, H. Wang, S. Kowarik, F. Schreiber, M. Paulus, M. Tolan, C. Sternemann, F. Evers, D. Zacher, R. A. Fischer and C. Wöll, *J. Am. Chem. Soc.*, 2007, **129**, 15118–15119.

20 A. Schoedel, C. Scherb and T. Bein, *Angew. Chem., Int. Ed.*, 2010, **49**, 7225–7228.

21 H. K. Arslan, O. Shekhah, J. Wohlgemuth, M. Franzreb, R. A. Fischer and C. Wöll, *Adv. Funct. Mater.*, 2011, **21**, 4228–4231.

22 V. Stavila, J. Volponi, A. M. Katzenmeyer, M. C. Dixon and M. D. Allendorf, *Chem. Sci.*, 2012, **3**, 1531.

23 K. Thürmer, C. Schneider, V. Stavila, R. W. Friddle, F. Léonard, R. A. Fischer, M. D. Allendorf and A. A. Talin, *ACS Appl. Mater. Interfaces*, 2018, **10**, 39400–39410.

24 F. Cheng, A. J. Young, J.-S. G. Bouillard, N. T. Kemp, R. Guillet-Nicolas, C. H. Hall, D. Roberts, A. H. Jaafar,

A. M. Adawi, F. Kleitz, A. Imhof, M. R. Reithofer and J. M. Chin, *J. Am. Chem. Soc.*, 2019, **141**, 12989–12993.

25 K. Ikigaki, K. Okada, Y. Tokudome, T. Toyao, P. Falcaro, C. J. Doonan and M. Takahashi, *Angew. Chem., Int. Ed.*, 2019, **58**, 6886–6890.

26 K. Ikigaki, K. Okada, Y. Tokudome and M. Takahashi, *J. Sol-Gel Sci. Technol.*, 2019, **89**, 128–134.

27 P. Falcaro, K. Okada, T. Hara, K. Ikigaki, Y. Tokudome, A. W. Thornton, A. J. Hill, T. Williams, C. Doonan and M. Takahashi, *Nat. Mater.*, 2017, **16**, 342–348.

28 K. Ikigaki, K. Okada and M. Takahashi, *ACS Appl. Nano Mater.*, 2021, **4**, 3467–3475.

29 K. Okada, M. Nakanishi, K. Ikigaki, Y. Tokudome, P. Falcaro, C. J. Doonan and M. Takahashi, *Chem. Sci.*, 2020, **11**, 8005–8012.

30 Q. Liu, J.-M. Yang, L.-N. Jin and W.-Y. Sun, *CrystEngComm*, 2016, **18**, 4127–4132.

31 O. Kwon, J. Y. Kim, S. Park, J. H. Lee, J. Ha, H. Park, H. R. Moon and J. Kim, *Nat. Commun.*, 2019, **10**, 3620.

32 A. Tarzia, M. Takahashi, P. Falcaro, A. W. Thornton, C. J. Doonan and D. M. Huang, *ACS Appl. Mater. Interfaces*, 2018, **10**, 40938–40950.

33 P. Falcaro, D. Buso, A. J. Hill and C. M. Doherty, *Adv. Mater.*, 2012, **24**, 3153–3168.

34 M. Tu, B. Xia, D. E. Kravchenko, M. L. Tietze, A. J. Cruz, I. Stassen, T. Hauffman, J. Teyssandier, S. De Feyter, Z. Wang, R. A. Fischer, B. Marmiroli, H. Amenitsch, A. Torvisco, M. D. J. Velásquez-Hernández, P. Falcaro and R. Ameloot, *Nat. Mater.*, 2021, **20**, 93–99.

35 P. Falcaro, A. J. Hill, K. M. Nairn, J. Jasieniak, J. I. Mardel, T. J. Bastow, S. C. Mayo, M. Gimona, D. Gomez, H. J. Whitfield, R. Riccò, A. Patelli, B. Marmiroli, H. Amenitsch, T. Colson, L. Villanova and D. Buso, *Nat. Commun.*, 2011, **2**, 237.

36 S. Hermes, F. Schröder, R. Chelmowski, C. Wöll and R. A. Fischer, *J. Am. Chem. Soc.*, 2005, **127**, 13744–13745.

37 C. M. Doherty, G. Grenci, R. Riccò, J. I. Mardel, J. Reboul, S. Furukawa, S. Kitagawa, A. J. Hill and P. Falcaro, *Adv. Mater.*, 2013, **25**, 4701–4705.

38 K. Okada, S. Sawai, K. Ikigaki, Y. Tokudome, P. Falcaro and M. Takahashi, *CrystEngComm*, 2017, **19**, 4194–4200.

39 T. Toyao, K. Liang, K. Okada, R. Ricco, M. J. Styles, Y. Tokudome, Y. Horiuchi, A. J. Hill, M. Takahashi, M. Matsuoka and P. Falcaro, *Inorg. Chem. Front.*, 2015, **2**, 434–441.

40 K. Okada, R. Ricco, Y. Tokudome, M. J. Styles, A. J. Hill, M. Takahashi and P. Falcaro, *Adv. Funct. Mater.*, 2014, **24**, 1969–1977.

41 H.-J. Son, S. Jin, S. Patwardhan, S. J. Wezenberg, N. C. Jeong, M. So, C. E. Wilmer, A. A. Sarjeant, G. C. Schatz, R. Q. Snurr, O. K. Farha, G. P. Wiederrecht and J. T. Hupp, *J. Am. Chem. Soc.*, 2013, **135**, 862–869.

42 J.-H. Dou, M. Q. Arguilla, Y. Luo, J. Li, W. Zhang, L. Sun, J. L. Mancuso, L. Yang, T. Chen, L. R. Parent, G. Skorupskii, N. J. Libretto, C. Sun, M. C. Yang, P. V. Dip, E. J. Brignole, J. T. Miller, J. Kong, C. H. Hendon, J. Sun and M. Dincă, *Nat. Mater.*, 2021, **20**, 222–228.